LETTERS

Contamination of the asteroid belt by primordial trans-Neptunian objects

Harold F. Levison[1,2], William F. Bottke[1,2], Matthieu Gounelle[3], Alessandro Morbidelli[4], David Nesvorný[1,2] & Kleomenis Tsiganis[5]

The main asteroid belt, which inhabits a relatively narrow annulus ~2.1–3.3 AU from the Sun, contains a surprising diversity of objects ranging from primitive ice–rock mixtures to igneous rocks. The standard model used to explain this assumes that most asteroids formed *in situ* from a primordial disk that experienced radical chemical changes within this zone[1]. Here we show that the violent dynamical evolution of the giant-planet orbits required by the so-called Nice model[2–4] leads to the insertion of primitive trans-Neptunian objects into the outer belt. This result implies that the observed diversity of the asteroid belt is not a direct reflection of the intrinsic compositional variation of the proto-planetary disk. The dark captured bodies, composed of organic-rich materials, would have been more susceptible to collisional evolution than typical main-belt asteroids. Their weak nature makes them a prodigious source of micrometeorites—sufficient to explain why most are primitive in composition and are isotopically different from most macroscopic meteorites[5,6].

Our result that a significant fraction of objects in the main asteroid belt are captured primordial trans-Neptunian objects (hereafter termed 'comets' or 'comet-like' to reflect their primitive, icy natures) comes from a series of numerical calculations of the trajectories of small bodies during dynamical events proposed in the Nice model[2,4]. In this model, the giant planets are assumed to have formed in a compact configuration (all were located between 5 and 15 AU from the sun) and to be surrounded by a ~$35M_\oplus$ disk of comet-like planetesimals stretching between ~16 and ~30 AU from the sun ($M_\oplus$ denoting the mass of the Earth). After roughly 600 Myr, the orbits of the giant planets became unstable. Uranus and Neptune were gravitationally scattered outwards, thereby penetrating the disk and scattering its constituents throughout the Solar System. The planets evolved into their current orbits as a result of the gravitational effects of the 'comets'. This model is unique because it can quantitatively explain many of the observed characteristics of the Solar System (for example giant-planet orbits[2], Trojan asteroids[2,7], the Kuiper belt[8], the irregular satellites[9] and the origin of the so-called late heavy bombardment[4]).

Our current simulations follow the dynamical evolution of objects that originally formed in the Nice model's primordial comet disk as the giant planets' orbits evolved. We are primarily interested in the fate of objects that potentially could have entered the inner Solar System. Thus, we first integrated the orbits of a large number of massless planetesimals initially on Saturn-crossing orbits under the gravitational influence of the Sun, Jupiter and Saturn. The planets were forced to migrate by including a suitably chosen acceleration in the planets' equations of motion, so that they reproduced the evolution of the 'fast migration' run in ref. 3 (see Supplementary

Information, section S1, for more details). During the integration, we supplied a steady flux of planetesimals through the Jupiter–Saturn system. These objects represent the planetesimals that originally formed in the trans-planetary disk, but were destabilized and fed inwards by Uranus and Neptune. The integrations covered 10 Myr. In all, we followed the evolution of ~31,000,000 disk particles. We find that a significant number of objects are captured either in Trojan orbits (as in ref. 3) or in orbits inside that of Jupiter. A Jupiter-crossing object can evolve into a stable orbit in the main asteroid belt through a combination of dynamical processes. Initially, Jupiter will scatter objects and occasionally one will fall in a mean-motion resonance, which can lower eccentricity. This would be temporary if there were no migration. With migration, however, the resonances move, and low-eccentricity objects can be left behind.

Next we tracked the long-term evolution of this captured comet-like population to compare it with observations. This population is affected by two processes: dynamical erosion and collisional grinding. To address the first, we integrated the orbits of the implanted comets under the gravitational effects of the Sun and gas giants for 4 Gyr. We removed an object if it either collided with a planet or reached a heliocentric distance greater than 15 AU or less than 1.5 AU. Figure 1 shows a comparison between the surviving objects (red dots) and a complete sample of known large asteroids (green pluses). We find that a substantial population of Trojans (32 of the 230 captured objects, or 13%) and Hilda asteroids (8%) are produced.

In addition, we captured comets in orbits in the main asteroid belt with semi-major axes as low as 2.68 AU. To compare these objects with the rest of the main belt, we used classification based on spectroscopy. According to our model, objects captured in the main belt should physically be similar to the resonant Trojans and Hildas. The vast majority of these resonant objects are classified as D- or P-type (hereafter D/P-type), which probably are organic-rich. Indeed, they are a good match to spectral characteristics of the observed dormant comets[10]. This is consistent with the Nice model's prediction that they formed beyond 15 AU.

The black dots in Fig. 1 show the D-type asteroids taken from the databases of refs 11, 12. There is reasonable agreement between the orbital element distribution of our captured objects and the known primitive asteroids (Trojans, Hildas and D-type main-belt objects). This result naturally leads to the controversial idea that most primitive asteroids formed beyond ~15 AU.

If the above model is correct, we need not only to be able to reproduce the orbits of the primitive, comet-like asteroids, but their total number and size distribution as well. To accomplish this, we need to account for their collisional evolution, which we do with a self-consistent code, CoDDEM, capable of following the collisional

[1]Southwest Research Institute, 1050 Walnut Street, Suite 300, [2]Center for Lunar Origin & Evolution, NASA Lunar Science Institute, Boulder, Colorado 80302, USA. [3]Laboratoire de Minéralogie et de Cosmochimie du Muséum, CNRS & Muséum National d'Histoire Naturelle, 75005 Paris, France. [4]Observatoire de la Côte d'Azur, Nice, Cedex 4, F-06304, France. [5]Department of Physics, Aristotle University of Thessaloniki, Thessaloniki, 54006 Hellas, Greece.
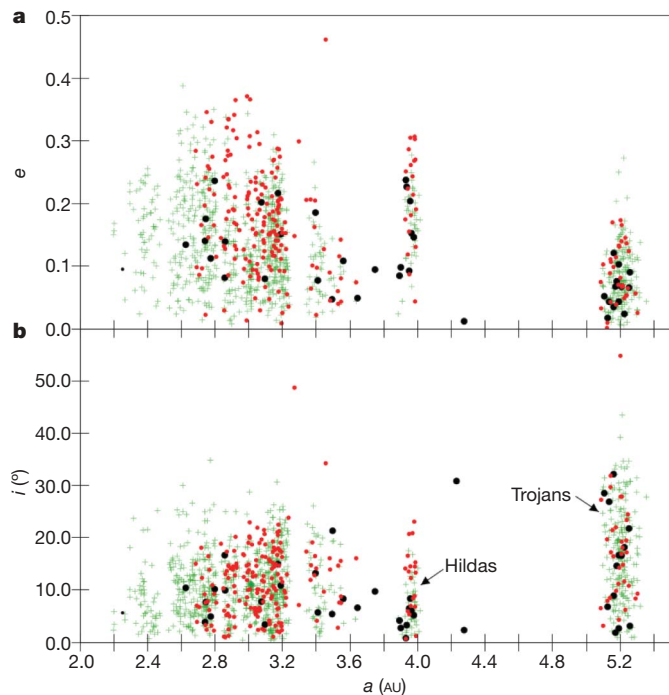
Figure 1 | The orbital element distributions of real and modelled asteroids. The distributions of eccentricity, e (**a**), and inclination, i (**b**), as functions of semi-major axis, a, of asteroids in Hilda (objects which orbit in the 2:3 mean-motion resonance with Jupiter near 3.9 AU), Trojan and main-belt populations. The small green pluses show all the numbered objects with diameters greater than 40 km (the asteroid belt is probably complete at these sizes) in the International Astronomical Union's Minor Planet Center database. We calculated the diameters from published absolute magnitudes, assuming the albedos (Supplementary Information, section S2.1). The black symbols show the D-type asteroids as catalogued in refs 11 and 12. It is important to note that asteroid (336) Lacadiera, at $a = 2.25$ AU, $e = 0.1$ and $i = 5.6°$, which is classified as a D-type in ref. 11, has an unusual spectrum (H. Campins, personal communication), and thus is probably a different type of object. We therefore use a smaller symbol to plot the location of this object and did not include it in our analysis. We only include D-type asteroids here because it is difficult to distinguish P-types from other, more processed, asteroids, with the result that the catalogue of P-types probably suffers from significant contamination[30]. The red dots show the location of objects captured during our simulations. The main result of our simulations is that, in addition to the resonant asteroids, a significant number of objects are trapped in the outer main belt (OMB). Unfortunately, it is not possible to perform a direct comparison between the orbital element distribution of our trapped objects and that of the D-types because the observations are biased owing to selection criteria, asteroid families and the like. However, we find noteworthy the fact that the inner edge of each populations is at $a \approx 2.6$ AU.

evolution and dynamical depletion of multiple interacting size-frequency distributions (SFDs)[13,14]. This code was modified to use an improved algorithm for handling the outcome of individual collisions, taken from ref. 15. We tracked five populations: (1) indigenous main-belt objects ($a < 2.82$ AU), (2) indigenous OMB objects, (3) captured OMB objects, (4) Hildas and (5) Trojans. The collision probabilities and impact velocities with both themselves and each other were computed from the observed objects or, in the case of the Trojans, were taken from refs 16–18. Populations 1 and 2, which represent native asteroids, had a bulk density of 2.7 g cm^{-3} and were assumed to follow the disruption scaling law for rocky objects[13]. We also assumed that the indigenous main-belt SFDs had approximately the same shape 3.9 Gyr ago as they do today[13,14].

The captured populations (3, 4 and 5) have a bulk density of 1 g cm^{-3}. We assumed that the initial shape of their SFDs was the same as that of the currently observed Trojans (Fig. 2 and Supplementary Information, section S2.2). Because the cometary disruption scaling law is not well understood, we performed four
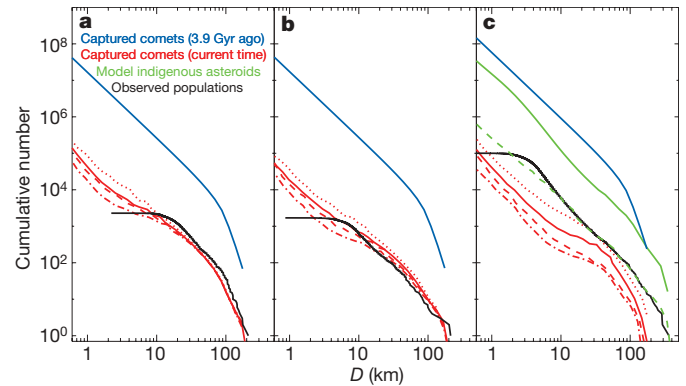

Figure 2 | The beginning and end states of the SFDs in the three regions studied. a, Trojans; **b**, Hildas; **c**, OMB objects. The blue curves show the initial conditions for the captured comets in our CoDDEM simulations. The shapes of the initial SFDs for these populations were taken from the currently observed Trojan SFD. We chose the Trojans because these objects have been least affected by collisional grinding. In particular, using the cumulative number $N(>D) \propto D^{-q}$, we assigned values of $q = 5.5$ for $D > 105$ km and $q = 1.8$ for $D < 105$ km, where D is diameter. The overall scales of the SFDs for the captured populations are derived from a combination of the observed Trojans and the results of the 10-Myr migration simulations (Supplementary Information, section S2.2). For each value of f_Q, we performed ~10 simulations using different random number generator seeds. The red curves show an average of these simulations and thus are our predictions for the present-day SFDs of the captured objects. In particular, the dotted, solid, dashed, and dash–dot red curves correspond to $f_Q = 1, 3, 5$ and 8, respectively. For the Hildas and Trojans, we expect the model SFD to match observations (black curves; note that the roll-off at small sizes is due to observational incompleteness). The agreement is quite good given the uncertainties in our models (Supplementary Information). Of particular note, the Trojans are known to have a significantly steeper SFD at $D \gtrsim 100$ km than the Hildas. Our model reproduces this because the Hildas, which cross the main belt, undergo more collisional grinding. For the main belt, the model also predicts that the SFD of the primitive bodies is steeper than that of the indigenous population for $D \gtrsim 20$ km, so the fraction of D/P-types should increase as diameter decreases. This appears to match observations[21]. The solid and dotted green curves in **c** refer to the indigenous OMB objects at the beginning and end of the simulation, respectively.

series of simulations in which this parameter was varied. In particular, following ref. 19, we assumed that the amount of energy required to catastrophically disrupt a comet is the same as that for solid ice[20], divided by a factor f_Q (Supplementary Information, section S2.2). We studied $f_Q = 1, 3, 5$ and 8 (the limit found in ref. 19). The required dynamical depletion rates were taken from the dynamical simulations described above, whereas those of the indigenous asteroids came from existing calculations of asteroid-belt depletion[4] in the Nice model (see the discussion about population 3 in Supplementary Information, section S1).

The results of our collisional calculations are shown in Fig. 2. Our model reproduces the SFDs of both the Trojan and Hilda populations for diameter $D > 40$ km fairly well. This agreement is important because each population has unique characteristics that test our model's assumptions. For example, comminution in the Trojan population comes mainly from members hitting one other, whereas that in the Hilda population is driven by impactors from across the asteroid belt. Matching the SFDs of these populations simultaneously in the same model, therefore, increases our confidence that our assumptions are reasonable.

The final state of the captured cometary OMB is strongly dependent on the disruption scaling laws used. For $f_Q = 1$, the model predicts that all of the OMB objects with $D > 40$ km are captured. For $f_Q = 3, 5$ and 8 we find that captured objects represent 48%, 20% and 16% of the OMB, respectively. This decrease is due to a much larger fraction of the captured objects being destroyed by impacts than their stronger indigenous counterparts. The best available bias-corrected

estimates of the fraction of D/P-types within the OMB over the same size range is ~20% (refs 21–23), suggesting that $f_Q \gtrsim 5$. Because the proportion of D/P-types is highly uncertain, this limit for f_Q is probably lower. The requirement that the primordial cometary disk survives the ~600 Myr before the late heavy bombardment requires that $f_Q < 5$ (Supplementary Information, section S4), which is consistent with our upper range. We conclude, therefore, that captured comets are weaker than native asteroids.

If the implanted comets are weaker than the indigenous main-belt asteroids, we can potentially resolve another long-standing problem in planetary science. The micrometeorites collected on the Earth are dominated by material reminiscent of carbonaceous chondrites. Indeed, the ratio of ordinary chondrite-type material to carbonaceous chondrite-type material (hereafter O/C) in micrometeorites is $\lesssim 0.16$ (ref. 24). Yet the asteroid belt, which has traditionally been considered the dominant source of this material[25] (see Supplementary Information, section S3, for alternatives), is roughly an equal mix of ordinary chondrite-like asteroids (for example S-types) and carbonaceous chondrite-like asteroids (for example C-types). The question has thus been that of why the micrometeorites we collect do not reflect this ratio.

In our successful collisional models (that is, those with $f_Q \geq 3$), we find that, at the current epoch, the implanted comets produce more than 15 times more dust per unit mass than the indigenous asteroids (the exact value depending on f_Q). This is because the implanted population is made up of weaker objects that are breaking up more easily. Furthermore, because the material created is mineralogically similar to that produced by primitive C-type asteroids, our model can explain the overabundance of carbonaceous chondrite micrometeorites. Indeed, collisional simulations of the current asteroid belt (Supplementary Information, section S3) show that an observed value of $O/C < 0.16$ is a common occurrence if $f_Q \geq 3$.

The idea that D/P-types are both weak and the source of micrometeorites also provides an explanation for the surprising fact that there are few micrometeorite analogues in our macroscopic meteorite collection. If we suppose that these micrometeorites are generated by the collisional cascade of embedded comets, we would not expect to see many macroscopic samples for two reasons. First, our implanted population resides in a region of the main belt from where it is very difficult to get meteorites[26,27]. In particular, macroscopic objects leaving this region of the asteroid belt are most likely to be ejected from the Solar System by Jupiter, whereas microscopic bodies, which are more susceptible to radiation forces, are more likely to be delivered to the Earth. In addition, the presumed weak nature of the captured objects probably makes their macroscopic fragments unlikely to survive the passage through the Earth's atmosphere or, if they do, survive for long on the Earth's surface.

Our conclusion that most primitive asteroids formed at large heliocentric distances and then were trapped in their current orbits, coupled with the idea that at least some asteroids were scattered into the main belt from the terrestrial-planet region[28], changes our view of the asteroid belt. The traditional interpretation of the diversity of the asteroid belt is that it represents the original condensation sequence in the protoplanetary disk[1]. Indeed, their orbital distribution has been used to constrain both the thermal structure of the nebula and the effectiveness of various heating mechanisms as a function of heliocentric distance (for example the decay of short-lived radionuclides such as ^{26}Al)[29]. If most D/P-types in the inner solar system were captured from farther out, however, our models of the protoplanetary disk would have to be significantly revised. Indeed, the diversity in the asteroid belt may be telling us more about the dynamical processes that controlled planet formation than about the physical nature of the protoplanetary nebula, with the main asteroid belt a collection point for rogue planetesimals from across the Solar System.

1. Bell, J. F., Davis, D. R., Hartmann, W. K. & Gaffey, M. J. in *Asteroids II* (eds Binzel, R. P., Gehrels, T. & Matthews, M. S.) 921–945 (Univ. Arizona Press, 1989).
2. Tsiganis, K., Gomes, R. S., Morbidelli, A. & Levison, H. F. Origin of the orbital architecture of the giant planets of the Solar System. *Nature* **435**, 459–461 (2005).
3. Morbidelli, A., Levison, H. F., Tsiganis, K. & Gomes, R. Chaotic capture of Jupiter's Trojan asteroids in the early Solar System. *Nature* **435**, 462–465 (2005).
4. Gomes, R. S., Levison, H. F., Morbidelli, A. & Tsiganis, K. Origin of the cataclysmic Late Heavy Bombardment period of the terrestrial planets. *Nature* **435**, 466–469 (2005).
5. Matrajt, G. *et al.* Oxygen isotope measurements of individual unmelted Antarctic micrometeorites. *Geochim. Cosmochim. Acta* **70**, 4007–4018 (2006).
6. Clayton, R. N. Oxygen isotopes in meteorites. *Annu. Rev. Earth Planet. Sci.* **21**, 115–149 (1993).
7. Nesvorný, D. & Vokrouhlický, D. Chaotic capture of Neptune Trojans. *Astron. J.* **137**, 5003–5011 (2009).
8. Levison, H. F., Morbidelli, A., Van Laerhoven, C., Gomes, R. & Tsiganis, K. Origin of the structure of the Kuiper belt during a dynamical instability in the orbits of Uranus and Neptune. *Icarus* **196**, 258–273 (2008).
9. Nesvorný, D., Vokrouhlický, D. & Morbidelli, A. Capture of irregular satellites during planetary encounters. *Astron. J.* **133**, 1962–1976 (2007).
10. Licandro, J., de León, J., Pinilla, N. & Serra-Ricart, M. Multi-wavelength spectral study of asteroids in cometary orbits. *Adv. Space Res.* **38**, 1991–1994 (2006).
11. Tholen, D. J. & Barucci, M. A. in *Asteroids II* (eds Binzel, R. P., Gehrels, T. & Matthews, M. S.) 298–315 (Univ. Arizona Press, 1989).
12. Bus, S. J. & Binzel, R. P. Phase II of the Small Main-Belt Asteroid Spectroscopic Survey. A feature-based taxonomy. *Icarus* **158**, 146–177 (2002).
13. Bottke, W. F. *et al.* The fossilized size distribution of the main asteroid belt. *Icarus* **175**, 111–140 (2005).
14. Bottke, W. F. *et al.* Linking the collisional history of the main asteroid belt to its dynamical excitation and depletion. *Icarus* **179**, 63–94 (2005).
15. Morbidelli, A., Bottke, W. F., Nesvorný, D. & Levison, H. F. Asteroids were born big. *Icarus*. (submitted).
16. Jewitt, D. C., Trujillo, C. A. & Luu, J. X. Population and size distribution of small Jovian Trojan asteroids. *Astron. J.* **120**, 1140–1147 (2000).
17. Yoshida, F. & Nakamura, T. Size distribution of faint Jovian L4 Trojan asteroids. *Astron. J.* **130**, 2900–2911 (2005).
18. Szabó, G. M., Ivezić, Ž., Jurić, M. & Lupton, R. The properties of Jovian Trojan asteroids listed in SDSS Moving Object Catalogue 3. *Mon. Not. R. Astron. Soc.* **377**, 1393–1406 (2007).
19. Leinhardt, Z. M. & Stewart, S. T. Full numerical simulations of catastrophic small body collisions. *Icarus* **199**, 542–559 (2009).
20. Benz, W. & Asphaug, E. Catastrophic disruptions revisited. *Icarus* **142**, 5–20 (1999).
21. Mothé-Diniz, T., Carvano, J. M. & Lazzaro, D. Distribution of taxonomic classes in the main belt of asteroids. *Icarus* **162**, 10–21 (2003).
22. Carvano, J. M., Mothé-Diniz, T. & Lazzaro, D. Search for relations among a sample of 460 asteroids with featureless spectra. *Icarus* **161**, 356–382 (2003).
23. Burbine, T. H. *et al.* Oxygen and asteroids. *Rev. Mineral. Geochem.* **68**, 273–343 (2008).
24. Genge, M. J. Ordinary chondrite micrometeorites from the Koronis asteroids. *Proc. Lunar Planet. Sci. Conf.* **37**, abstr. 1759 (2006).
25. Dermott, S. F., Durda, D. D., Grogan, K. & Kehoe, T. J. J. in *Asteroids III* (eds Bottke, W. F., Paolicchi, P., Binzel, R. P. & Cellino, A.) 423–442 (Univ. Arizona Press, 2002).
26. Morbidelli, A. & Gladman, B. Orbital and temporal distributions of meteorites originating in the asteroid belt. *Meteorit. Planet. Sci.* **33**, 999–1016 (1998).
27. Bottke, W. F. Jr, Rubincam, D. P. & Burns, J. A. Dynamical evolution of main belt meteoroids: numerical simulations incorporating planetary perturbations and Yarkovsky thermal forces. *Icarus* **145**, 301–331 (2000).
28. Bottke, W. F., Nesvorný, D., Grimm, R. E., Morbidelli, A. & O'Brien, D. P. Iron meteorites as remnants of planetesimals formed in the terrestrial planet region. *Nature* **439**, 821–824 (2006).
29. Grimm, R. E. & McSween, H. Y. Heliocentric zoning of the asteroid belt by aluminum-26 heating. *Science* **259**, 653–655 (1993).
30. Clark, B. E., Rivkin, A. S., Bus, S. J., Sanders, J. & X. E, M, and P-type asteroid spectral observations. *Bull. Am. Astron. Soc.* **35**, 955 (2003).